IOP PUBLISHING JOURNAL OF PHYSICS: CONDENSED MATTER

J. Phys.: Condens. Matter **22** (2010) 465306 (9pp) doi:10.1088/0953-8984/22/46/465306

Calculation of transmission probability by solving an eigenvalue problem

Sergiy Bubin and Kálmán Varga

Department of Physics and Astronomy, Vanderbilt University, Nashville, TN 37235, USA

Received 19 May 2010, in final form 15 September 2010
Published 5 November 2010
Online at stacks.iop.org/JPhysCM/22/465306

Abstract

The electron transmission probability in nanodevices is calculated by solving an eigenvalue problem. The eigenvalues are the transmission probabilities and the number of nonzero eigenvalues is equal to the number of open quantum transmission eigenchannels. The number of open eigenchannels is typically a few dozen at most, thus the computational cost amounts to the calculation of a few outer eigenvalues of a complex Hermitian matrix (the transmission matrix). The method is implemented on a real space grid basis providing an alternative to localized atomic orbital based quantum transport calculations. Numerical examples are presented to illustrate the efficiency of the method.

(Some figures in this article are in colour only in the electronic version)

1. Introduction

The investigation of electronic transport properties of nanoscale materials is at the center of experimental and theoretical research. Quantum transport calculations [1–14] are developing at a very fast pace. Most quantum transport calculations are based on the nonequilibrium Green's function (NEGF) formalism with density functional theory (DFT) Hamiltonians, and most implementations of these calculations use localized atomic orbitals as basis sets.

Real space mesh [15–18] approaches are very popular and powerful basis sets in density functional calculations but their application in transport calculations is limited [14, 19–21]. In the following, we refer to these bases as grid bases (as they are defined on a grid in real or reciprocal space) to distinguish them from localized atomic orbitals. These grid basis sets provide an alternative to localized atomic orbitals in quantum transport calculations. The grid basis functions are evenly distributed in space and not tied to atomic positions. The real space grid provides a flexible representation of rapidly oscillating current carrying states. In a recent paper [22] we have shown that the nonlocalized grid type basis functions provide accurate results for transport properties. The basis size in the grid calculations, however, is so large that the NEGF formalism cannot be easily implemented using grid basis functions. Grid basis calculations therefore have to calculate the scattering wavefunction explicitly by using the transfer-matrix [23], Lippmann–Schwinger, or complex band structure [24] approaches. Once the scattering wavefunction is available the transmission probability can be calculated. The scattering wavefunction based approaches work well but are generally slower and their implementation is more complicated than that of the NEGF formalism.

One of the most important advantages of the NEGF approach is that once the Hamiltonian and overlap matrices are available in a suitable basis function representation, the formalism only includes matrix linear algebra in an elegant and straightforward manner. For ballistic transport, the transmission as a function of energy is calculated from a trace expression,

$$T(E) = \mathrm{Tr}(\mathcal{T}), \qquad \mathcal{T} = G_{\mathrm{C}}\Gamma_{\mathrm{L}}G_{\mathrm{C}}^{\dagger}\Gamma_{\mathrm{R}}, \tag{1}$$

where G_{C} is the Green's function of the device, and Γ_{L} and Γ_{R} are the imaginary parts of the self-energy matrices. This expression can be evaluated provided that the size of these matrices is manageable. In the case of a grid calculation, as noted earlier, this is not the case because the dimension of the device's Green's function can easily be several hundreds of thousands. The Hamiltonian in grid calculations is sparse but the Green's function is a dense matrix, which makes the calculation prohibitively expensive. Note that to calculate the transmission, one does not need to calculate all the elements of the Green's function, only those matrix elements are needed which are connected to the Γ_{L} and Γ_{R} broadening matrices. The number of those matrix elements is, however, still too large to make the formation of the transmission matrix and calculation of the trace manageable. One can try to calculate the transmission by evaluating the trace by Monte Carlo

sampling [25]. The Monte Carlo approach, however, has a statistical error associated with it and is not very efficient.

In this paper we propose a different approach to evaluate the trace in equation (1). Instead of calculating the trace directly from matrix $\mathcal{T}$, $\mathcal{T}$ is diagonalized first and the trace is calculated from the eigenvalues. At first glance this seems to be more complicated than the direct evaluation but it is not. The $\mathcal{T}$ matrix has only a few nonzero eigenvalues T_i [26] and instead of diagonalizing $\mathcal{T}$ one can diagonalize $\mathcal{T}^{-1}$ and calculate the eigenvalues $1/T_i$. This is the key advantage of this approach. In the inverse of $\mathcal{T}$, in place of the dense Green's function one has the sparse Hamiltonian, and the diagonalization amounts to roughly the same amount of computational effort as the diagonalization of the Hamiltonian in the ground state DFT calculations. Moreover, one only needs to find the lowest few eigenvalues of $\mathcal{T}^{-1}$ and efficient iterative diagonalization approaches such as the Lanczos or the Krylov subspace methods can be used.

In this paper we will restrict ourselves to zero bias calculations. The self-consistent potential is obtained by solving the Kohn–Sham equations on a real space grid. The electron density is calculated from the Kohn–Sham orbitals, that is the computationally expensive calculation of the density from the Green's function on a real space grid, $\rho = -\frac{1}{\pi}\,\mathrm{Im}(G_\mathrm{C})$, is avoided. The presented approach allows the calculation of the transmission probability directly from the results of a conventional ground state type real space calculation using the simple NEGF trace formula without the extra burden of computing the scattering states. We will present several numerical examples to illustrate the proposed approach.

The approach proposed in this work shares the same spirit as the approach presented in [26]. In [26] the authors have calculated the transmission eigenchannels of the leads avoiding the need for the tedious calculation of the scattering states in the leads. In this work we have presented a method in which the calculation of the scattering states is bypassed by solving the eigenvalue problems of the transmission matrix.

The outline of this paper is as follows. In section 2 we introduce the main points of the formalism. In section 3 we present numerical examples to show the applicability of the method. This is followed by a brief summary. Some of the important details of the approach are presented as appendices.

2. Formalism

2.1. Preliminaries

In the NEGF framework the system is divided into left and right leads and a device part as shown in figure 1. The leads consist of periodically repeated layers (boxes). The Hamiltonian is defined as

$$H_\mathrm{KS} = -\frac{\hbar^2}{2m}\nabla^2 + V_\mathrm{A}(\mathbf{r}) + V_\mathrm{H}[\rho](\mathbf{r}) + V_\mathrm{xc}[\rho](\mathbf{r}), \qquad (2)$$

where V_A is the Coulomb potential of the atomic nuclei, V_H is the Hartree potential, and V_xc is the exchange–correlation potential.

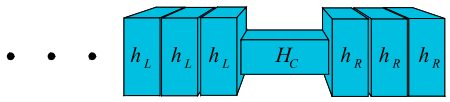

Figure 1. Organization of the system into left/right leads (L/R) and a central device (C). The self-consistent potential is calculated for the central region. Only a few layers of the leads need to be included to obtain a converged potential for the central region.

Each region is represented by a set of basis functions $\{\Psi_i^\mathrm{L}\}_{i=1}^{N_\mathrm{L}}$, $\{\Psi_i^C\}_{i=1}^{N_\mathrm{C}}$ and $\{\Psi_i^\mathrm{R}\}_{i=1}^{N_\mathrm{R}}$. $N_\mathrm{L}, N_\mathrm{C}$ and N_R are the numbers of basis functions in the left, center and right regions. The functions Ψ_i^L, Ψ_i^C and Ψ_i^R are centered at the left, center and right regions, respectively. The dimension of the basis describing the left and right semi-infinite leads is infinite. To make the calculations feasible, we add a complex absorbing potential (CAP) to the left and to the right semi-infinite leads. These complex potentials transform the open infinite system into a closed finite system by effectively cutting off the leads beyond a certain distance. Test calculations presented in [27] show that the CAP approach gives the same results as the direct calculation using infinite leads. The details of the CAP approach are given in appendix A. As a result of the addition of the CAP in the leads the dimension N_L (N_R) of the left (right) basis is finite.

An orthonormal set of basis states is used in the calculations:

$$\langle\Psi_i^X|\Psi_j^Y\rangle = \delta_{ij}\delta_{XY}, \qquad Y = L, C, R, \qquad (3)$$

but one can generalize the formalism to nonorthogonal basis functions without difficulty. The basis functions will be defined in the next subsection.

In this basis representation the Hamiltonian matrix of the left-lead–device–right-lead system, under the assumption that there is no interaction between the leads, takes the form

$$H = \begin{pmatrix} H_\mathrm{L} & H_\mathrm{LC} & 0 \\ H_\mathrm{LC}^\dagger & H_\mathrm{C} & H_\mathrm{RC}^\dagger \\ 0 & H_\mathrm{RC} & H_\mathrm{R} \end{pmatrix},$$

where H_L, H_C, and H_R are the Hamiltonian matrices of the leads and the device. H_LC and H_RC are the coupling matrices between the central region and the leads defined as

$$(H_{XY})_{ij} = \langle\Psi_i^X|H_\mathrm{KS}|\Psi_j^Y\rangle. \qquad (4)$$

Using this Hamiltonian, the transmission coefficient can be calculated by the standard NEGF formalism [1]. In the framework of the NEGF approach, the transmission coefficient can be calculated using the self-energies of the leads and the Green's functions of the center region. These quantities are defined as follows. The broadening matrices of the leads ($X = \mathrm{L}, \mathrm{R}$) are given by the expression

$$\Gamma_X(E) = \mathrm{i}(\Sigma_X(E) - \Sigma_X^\dagger(E)), \qquad (5)$$

where

$$\Sigma_X(E) = H_{XC}^\dagger\, g_X(E) H_{XC} \qquad (6)$$

and

$$g_X(E) = ((E + i\epsilon^+)I_X - H_X)^{-1} \tag{7}$$

is the Green's function of the semi-infinite leads. I_X is the unit matrix in the $X = \mathrm{L}, \mathrm{R}$ region and ϵ^+ is an infinitesimally small positive number. The Green's function of the central region is

$$G_\mathrm{C}(E) = ((E + \mathrm{i}\epsilon^+)I_\mathrm{C} - H_\mathrm{C} - \Sigma_\mathrm{L}(E) - \Sigma_\mathrm{R}(E))^{-1}, \tag{8}$$

where I_C is the unit matrix in the central region. The transmission probability is given by [1]

$$T(E) = \mathrm{Tr}(\mathcal{T}) \qquad \mathcal{T} = G_\mathrm{C}(E)\Gamma_\mathrm{L}(E)G_\mathrm{C}(E)^\dagger\Gamma_\mathrm{R}(E). \tag{9}$$

In this equation the transmission coefficient, $T(E)$, is expressed through the Green's function of the device and the semi-infinite leads. The Green's functions of the semi-infinite leads, g_X, can be calculated by the decimation technique [28], but in this work we use a different approach by adding complex absorbing potentials to the lead Hamiltonian (see appendix A).

To calculate $\mathcal{T}$ one needs to have the Green's function of the central region, $G_\mathrm{C}(E)$, and broadening matrices, $\Gamma_X(E)$. Both of these are $N_\mathrm{C} \times N_\mathrm{C}$ matrices, where N_C is the dimension of the basis (the number of grid points) in the central region. As is shown in appendix A, the broadening matrices are sparse matrices with only a small nonzero block matrix. Using this simplification, the trace formula can be written as

$$T(E) = \sum_{j=1}^{m_\mathrm{L}} \sum_{k=1}^{m_\mathrm{L}} \sum_{l=N_\mathrm{C}-m_\mathrm{R}+1}^{N_\mathrm{C}} \sum_{m=N_\mathrm{C}-m_\mathrm{R}+1}^{N_\mathrm{C}} (G_\mathrm{C}(E))_{mj} \times (\Gamma_\mathrm{L}(E))_{jk}(G_\mathrm{C}(E)^\dagger)_{kl}(\Gamma_\mathrm{R}(E))_{lm}, \tag{10}$$

where m_L and m_R are the dimensions of the nonzero block matrices of Γ_L and Γ_R (see appendix A.). Although the number of matrix elements to be calculated has been reduced by exploiting the sparsity of the broadening matrices, the direct evaluation of the sum is still prohibitively expensive as we will show in the numerical examples section. To avoid the calculation of $G_\mathrm{C}(E)$ which is a dense matrix we calculate $T(E)^{-1}$ which only contains sparse matrices as we will show in section 2.3.

2.2. Basis functions

In this subsection we describe the basis functions of the calculations. A real space mesh using Lagrange functions [18] will be used to represent the Hamiltonian. The basis functions are tensorial products of one-dimensional Lagrange functions [18]:

$$\Psi_i(x, y, z) = \Psi_{\alpha\beta\gamma}(x, y, z) = L_\alpha(x)L_\beta(y)L_\gamma(z). \tag{11}$$

These basis functions are defined on a three-dimensional mesh in the computational cell $[a_x, b_x] \times [a_y, b_y] \times [a_z, b_z]$. The mesh points are

$$\mathbf{r}_i = (x_\alpha, y_\beta, z_\gamma) \tag{12}$$

where $\alpha = 1, \ldots, N_x$, $\beta = 1, \ldots, N_y$, $\gamma = 1, \ldots, N_z$ and N_x, N_y and N_z are the numbers of mesh points in the x, y and z directions. The basis function $\Psi_{\alpha\beta\gamma}$ is only nonzero on the $i = (\alpha\beta\gamma)$ grid point and zero on all other grid points.

In the $[a_x, b_x]$ interval in the x direction, the basis function is

$$L_\alpha(x) = \frac{2}{N_x + 1} \sum_{k=1}^{N_x} \sin\left(k\pi \frac{x - a_x}{b_x - a_x}\right) \sin\left(k\pi \frac{x_\alpha - a_x}{b_x - a_x}\right), \tag{13}$$

with equally spaced grid points

$$x_\alpha = a_x + \frac{b_x - a_x}{N_x + 1}\alpha \qquad \alpha = 1, \ldots, N_x. \tag{14}$$

This basis function is zero at the boundaries $L_\alpha(a_x) = L_\alpha(b_x) = 0$.

The Lagrange functions are orthogonal

$$\int_{a_x}^{b_x} L_\alpha(x)L_{\alpha'}(x) = \lambda_\alpha \delta_{\alpha\alpha'}, \tag{15}$$

form a complete set of states and the results of the calculations converge exponentially with respect to the number of grid points [29]. They have the property

$$L_\alpha(x_\nu) = \delta_{\alpha\nu}, \tag{16}$$

that is each basis function is nonzero only at one grid point.

In the perpendicular y and z directions we use a periodic Lagrange basis

$$L_\beta(y) = \frac{1}{N} \sum_{k=1}^{N_y} \cos[\pi(2k - N - 1)(y - y_\beta)] \tag{17}$$

where

$$y_\beta = \frac{a_y + b_y}{2} + \frac{b_y - a_y}{N_y}\beta \qquad \beta = 1, \ldots, N_y \tag{18}$$

are equidistant grid points. This basis function is periodic, $L_\beta(a_y) = L_\beta(b_y)$. The basis functions in the z directions are defined analogously to $L_\beta(y)$. The most important property of these basis functions is that, similar to the finite difference approach, the potential energy matrix is diagonal. The nonlocal pseudopotential matrix elements are short ranged and connect only a few neighboring grid points. The kinetic energy matrix elements are truncated if the distance between two grid points is larger than a preset value. These matrix elements can be neglected without losing accuracy [18]. The Hamiltonian matrix is, therefore, block tridiagonal in this representation.

The computational cell in the x direction is divided into regions. The center region starts at c_L and ends at c_R. The left region contains the grid points $a_x \leqslant x_\alpha < c_\mathrm{L}$ and the basis functions in that region are labeled as

$$\Psi^\mathrm{L}(x, y, z) = \Psi_{\alpha\beta\gamma}(x, y, z) \qquad a_x \leqslant x_\alpha < c_\mathrm{L}. \tag{19}$$

Ψ_i^C and Ψ_i^R are defined similarly. In the center one has

$$\Psi^C(x, y, z) = \Psi_{\alpha\beta\gamma}(x, y, z) \qquad c_\mathrm{L} \leqslant x_\alpha \leqslant c_\mathrm{R} \tag{20}$$

and in the right region the basis functions are labeled as

$$\Psi^\mathrm{R}(x, y, z) = \Psi_{\alpha\beta\gamma}(x, y, z) \qquad c_\mathrm{R} < x_\alpha \leqslant b_x. \tag{21}$$

The matrix elements of the Hamiltonian, defined in section 2.1, are calculated using these basis functions. The approach is not limited to these basis functions; other localized functions, for example a finite difference grid or finite elements, could also be used. Note that we will use a complex absorbing potential in the leads which effectively cuts off the leads at finite distances. Therefore the fact that the basis functions are zero at the boundaries (at a_x and b_x) in the x-direction does not affect the calculation.

2.3. Formulating an eigenvalue problem

By defining

$$t(E) = \Gamma_{\mathrm{L}}(E)^{1/2} G_{\mathrm{C}}(E) \Gamma_{\mathrm{R}}(E)^{1/2} \tag{22}$$

and using the cyclic property of the trace, $\mathcal{T}(E)$ can be written [30] in the Landauer form

$$T(E) = \mathrm{Tr}(t(E)t^{\dagger}(E)). \tag{23}$$

The existence of the real matrix $\Gamma_X^{1/2}$ is guaranteed because Γ_X is a positive definite matrix [30]. The matrix $t(E)t^{\dagger}(E)$ is a Hermitian matrix having real eigenvalues T_i bounded by $0 \leqslant T_i \leqslant 1$. Although the dimension of $t(E)t^{\dagger}(E)$ is arbitrarily large depending on the basis representation of the device region, the number of nonzero eigenvalues is limited to the actual number of conducting channels given by $M = \min(M_{\mathrm{L}}(E), M_{\mathrm{R}}(E))$ [31, 32] (where $M_{\mathrm{L}}(E)$ is the number of incoming channels in the left and $M_{\mathrm{R}}(E)$ is the number of outgoing channels in the right at energy E). The calculation of the transmission probability amounts to determining the nonzero eigenvalues of $\mathcal{T}$.

Matrix $\mathcal{T}$ contains the Green's functions which are dense matrices even if the Hamiltonian itself is sparse. Therefore the direct calculation of the eigenvalues is not practical. One can determine the eigenvalues of $\mathcal{T}^{-1}$ instead. The inverse matrix is defined as

$$\begin{aligned}\mathcal{T}^{-1} &= \Gamma_{\mathrm{R}}(E)^{-1} G_{\mathrm{C}}(E)^{\dagger-1} \Gamma_{\mathrm{L}}(E)^{-1} G_{\mathrm{C}}(E)^{-1} \\ &= \Gamma_{\mathrm{R}}(E)^{-1}[(E - \mathrm{i}\epsilon^{+} - H_{\mathrm{C}} - \Sigma_{\mathrm{L}}(E)^{\dagger} - \Sigma_{\mathrm{R}}(E)^{\dagger})] \\ &\quad \times \Gamma_{\mathrm{L}}(E)^{-1}[E + i\epsilon^{+} - H_{\mathrm{C}} - \Sigma_{\mathrm{L}}(E) - \Sigma_{\mathrm{R}}(E)].\end{aligned} \tag{24}$$

In this equation,

$$E + \mathrm{i}\epsilon^{+} - H - \Sigma_{\mathrm{L}}(E) - \Sigma_{\mathrm{R}}(E) \tag{25}$$

is sparse (except for the small corner matrices $\Sigma_{\mathrm{L}}(E)$ and $\Sigma_{\mathrm{R}}(E)$ as is discussed in appendix B). The eigenvalues of $\mathcal{T}^{-1}$ are $\frac{1}{T_i}$. The M nonzero eigenvalues of $\mathcal{T}$ become the M lowest eigenvalues of $\mathcal{T}^{-1}$, while all other eigenvalues become infinite. Iterative diagonalization approaches, particularly the Lanczos method, are very suitable for calculating the desired lowest eigenvalues. The application of the Lanczos method in the present case is described in appendix B.

To make these calculations feasible one has to avoid the infinite-dimensional matrices of the semi-infinite leads. This can be achieved by adding a complex absorbing potential (CAP) into the leads [27]. The CAP transforms the infinite lead into a finite system and the sparse matrix algebra described above can now be implemented easily. As is shown in [27], the self-energy matrices calculated by direct evaluation in the infinite system and by using the CAP approach are the same. The implementation of the CAP in the present calculation is described in appendix A.

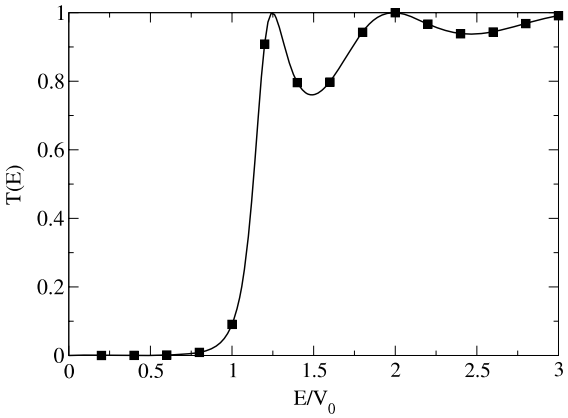

Figure 2. Transmission probability for a one-dimensional rectangular potential barrier. The solid line is the analytical solution and the squares are obtained by solving the eigenvalue problem. The barrier height is $V_0 = 5$, the barrier width is $a = 2$ and $\hbar^2/m = 1$.

3. Numerical results

As a first test example we calculate the transmission probability as a function of energy for scattering on a rectangular potential barrier in one dimension. The result of the eigenvalue calculation is compared to the analytical solution in figure 2. The agreement is perfect showing that the method works very well. As this is a one-dimensional problem, there is only one incoming and outgoing wave for each energy so matrix $\mathcal{T}$ has only one nonzero eigenvalue.

The second example is the calculation of the transmission coefficient of a linear monoatomic chain of gold atoms placed at a distance of 2.9 Å from each other. A unit cell containing three gold atoms was used in the calculations. The transmission in this monoatomic wire is equal to $n \times G_0$ where n is the number of open channels and $G_0 = 2e^2/h$ is the unit of the quantum conductance. Figure 3 shows the quantized transmission as a function of energy. Each channel has unit conductance, that is the nonzero eigenvalues are $T_i = 1$. For this system, the number of eigenvalues times G_0 is equal to the transmission probability $T(E)$. Figure 3 also shows the density of states and the band structure of the monoatomic gold wire. One can see clear correlation between the electronic structure and the transmission coefficient. The lowest band starts somewhat below -3.1 eV and the transmission in zero below that threshold. Once a Bloch state becomes available the transmission is equal to one. As the energy increases, at around $E = -2.2$ eV there is a small spike in the transmission coinciding with the position of the edge of the Brillouin zone. Increasing the energy further at around $E = -1.5$ eV a second transmission channel opens up (two Bloch states become accessible) and a sharp increase appears in the density of states. Next, at the edge of the Brillouin zone at $E = -1.2$ eV and $k = 0$ there is a sharp drop in the transmission with a noticeable

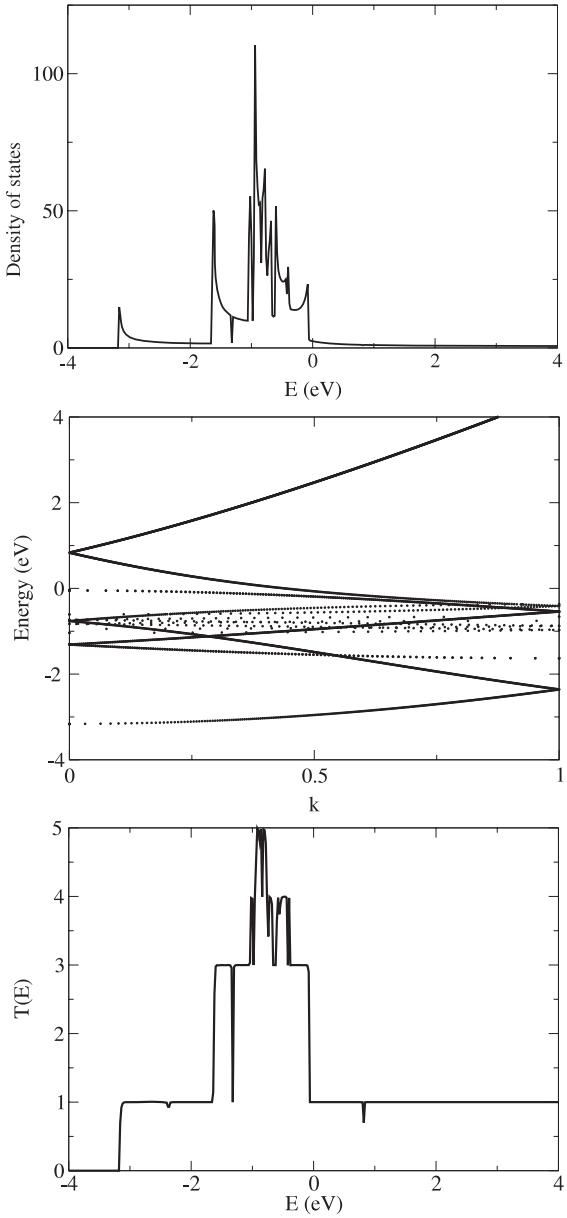

Figure 3. Density of states in arbitrary units (top), band structure (middle) and transmission probability (bottom) of a monoatomic gold chain. The wave number k is in units of π/L in the band structure plot (L is the lattice constant of the unit cell).

spike in the density of states. The rest of the results presented in figure 3 follow a similar tendency. The transmission, density of state and the band structure are clearly related.

As a next test we add a CO molecule to the middle atom of the chain. The coordinates of the C and O atoms are the same as in [33, 22]. The CO adsorbate completely changes the transmission probability. This system has been studied earlier by several groups [34, 33, 22] and serves as a benchmark for transport calculations. Our results, presented in figure 4, agree very well with the results of [33]. Due to the scattering on the perturbation potential of the CO adsorbate the nonzero transmission eigenvalues are not equal to one anymore, but the number of nonzero eigenvalues (the number of open channels in the leads for a given energy) remains the same.

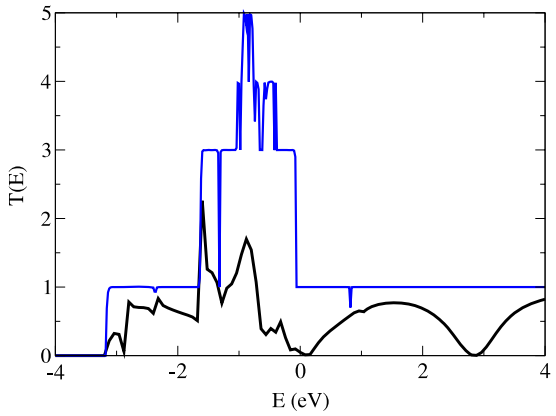

Figure 4. Transmission probability (lower thick line) for a CO molecule adsorbed onto a gold chain. The transmission of an unperturbed monoatomic wire (higher thin line) is shown for comparison.

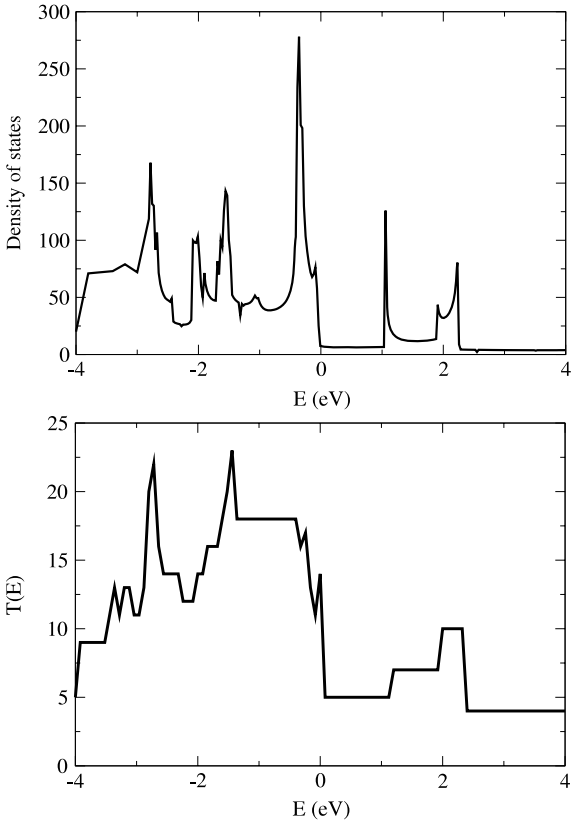

Figure 5. Density of states in arbitrary units (top) and transmission probability (bottom) for a bulk gold electrode.

To test the method on a larger system we have calculated the transmission probability in perfect gold electrodes. The lattice parameter of the bulk gold used in the calculation is 4.18 Å. The calculated density of states and transmission probability is shown in figure 5. The changes in the density of states and the steps and spikes in the transmission are in correlation, similarly to the case of the monoatomic gold wire in figure 3.

As a next example we separate the system into left and right leads and place a three atom gold chain between the

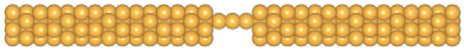

Figure 6. Monoatomic gold wire between gold electrodes.

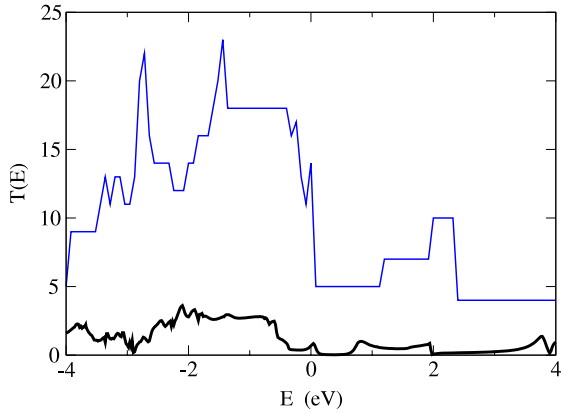

Figure 7. Transmission probability (lower thick line) for a monoatomic gold constriction placed between gold electrodes. The transmission of the gold electrode (higher thin line) is shown for comparison.

leads as shown in figure 6. The distance between the gold atoms is 2.9 Å and the distance between the gold atoms and the lead is also 2.9 Å. Figure 7 compares the transmission in the lead–wire–lead system to the transmission in the perfect lead obtained in the previous example, see figure 5. The figure shows that the number of nonzero eigenvalues (which is equal to the transmission in the perfect lead) remains the same but the eigenvalues are not equal to one anymore. The transmission probability changes dramatically due to electron scattering on the gold chain constriction. Placing a molecule or any other system between the gold electrodes would give similar results. The calculated transmission would obviously change but the number of nonzero eigenvalues to be calculated would remain the same.

Table 1 shows the number of nonzero eigenvalues for the systems studied. The table illustrates that while the basis dimension is large, the number of eigenvalues to be calculated is small making this approach an efficient alternative to the conventional trace calculation.

Table 1 also shows the dimension of the nonzero block matrix of the broadening matrices. In the case of the 1d square well potential m_{L} corresponds to the range of the kinetic energy (beyond that range the kinetic energy matrix is zero). In the three-dimensional test cases $m_{\mathrm{L}} = m \times N_y \times N_z$, where m is determined by the range of the pseudopotential ($m_{\mathrm{R}} = m_{\mathrm{L}}$ for identical leads). The direct evaluation of the trace using (9) would require the calculation of $m_{\mathrm{L}} \times m_{\mathrm{L}}$ elements of G_{C} which is clearly prohibitively expensive.

4. Summary

Real space mesh calculations are very popular and powerful. The application of these approaches to transport calculations in the simple and elegant Green's function framework, however, is not easy due to the need for the computationally expensive evaluation of the trace expression of the transmission probability. In this paper the trace calculation of the transmission probability is re-cast into an eigenvalue problem of $\mathcal{T}(E)$. Only a few of the eigenvalues of this matrix are nonzero and these eigenvalues can be calculated very efficiently with the Lanczos method using sparse matrix operations. This approach avoids the difficulties associated with the calculation of the Green's function needed in the direct evaluation of the trace allowing the calculation of the transmission probability using the trace formula in grid type basis calculations. This makes the grid calculations simpler because the scattering wavefunction does not need to be explicitly calculated to determine the transmission probability.

The numerical test examples presented in this paper illustrate the efficiency of the method.

Table 1. Maximum number of nonzero eigenvalues M in the $[E_{\mathrm{F}} - 4\ \mathrm{eV}, E_{\mathrm{F}} + 4\ \mathrm{eV}]$ energy range (E_{F} is the Fermi energy). N_{C} is the number of grid points in the central region, m_{L} is the number of nonzero elements of the broadening matrices.

System	M	N_{C}	m_{L}
1d square well	1	50	4
Gold wire	5	280 908	18 491
Gold lead	23	436 590	14 993

Acknowledgments

This work is supported by NSF grants SCCS0925422 and CMMI0927345.

Appendix A. Transport calculation with complex absorbing potentials

In the conventional NEGF approach using an appropriate basis representation the Hamiltonian matrix has a block-tridiagonal structure

$$H = \begin{pmatrix} H_{\mathrm{L}} & H_{\mathrm{LC}} & 0 \\ H_{\mathrm{LC}}^{\dagger} & H_{\mathrm{C}} & H_{\mathrm{RC}}^{\dagger} \\ 0 & H_{\mathrm{RC}} & H_{\mathrm{R}} \end{pmatrix}. \tag{26}$$

In the derivation of this Hamiltonian one has to assume that the basis functions are suitable short ranged ones and the left and the right leads are not connected by the basis functions, that is the right upper and the left bottom corner are zero. The Hamiltonians of the right and the left leads are

$$H_{\mathrm{R}} = \begin{pmatrix} h_{00}^{R} & h_{10}^{R\dagger} & 0 & \dots & 0 & 0 \\ h_{10}^{R} & h_{00}^{R} & h_{10}^{R\dagger} & \dots & 0 & 0 \\ 0 & h_{10}^{R} & h_{00}^{R} & \dots & 0 & 0 \\ \vdots & \vdots & \vdots & \ddots & \vdots & \vdots \\ 0 & 0 & 0 & \dots & h_{00}^{\mathrm{R}} & h_{10}^{R\dagger} \\ 0 & 0 & 0 & \dots & h_{10}^{\mathrm{R}} & h_{00}^{\mathrm{R}} \end{pmatrix}, \tag{27}$$

$$H_{\mathrm{L}} = \begin{pmatrix} h_{00}^{L} & h_{10}^{L\dagger} & 0 & \dots & 0 & 0 \\ h_{10}^{L} & h_{00}^{L} & h_{10}^{L\dagger} & \dots & 0 & 0 \\ 0 & h_{10}^{L} & h_{00}^{L} & \dots & 0 & 0 \\ \vdots & \vdots & \vdots & \ddots & \vdots & \vdots \\ 0 & 0 & 0 & \dots & h_{00}^{\mathrm{L}} & h_{10}^{L\dagger} \\ 0 & 0 & 0 & \dots & h_{10}^{\mathrm{L}} & h_{00}^{\mathrm{L}} \end{pmatrix}, \quad (28)$$

where the block-tridiagonal structure is due to the fact that the lead is made of periodically repeated 'principal layers' and the basis functions only connect the neighboring layers. In the present work the Lagrange functions are localized at grid points, the local potential is diagonal in this representation. The pseudopotential matrix elements are nonzero only within the radius of the local pseudopotential. The local pseudopotential is short ranged so only the adjacent layers are connected with the basis functions. The kinetic energy is also a sparse matrix which can be truncated so that only adjacent layers are connected. The Lagrange basis thus leads to the above block-tridiagonal representation. The coupling matrices between the leads and the central region are

$$H_{\mathrm{LC}} = \begin{pmatrix} 0 & 0 & \dots & 0 \\ 0 & 0 & \dots & 0 \\ 0 & 0 & \dots & 0 \\ \vdots & \vdots & \ddots & \vdots \\ 0 & 0 & \dots & 0 \\ h_{\mathrm{LC}} & 0 & \dots & 0 \end{pmatrix}, \quad (29)$$

$$H_{\mathrm{RC}} = \begin{pmatrix} 0 & \dots & 0 & h_{\mathrm{RC}} \\ 0 & \dots & 0 & 0 \\ 0 & \dots & 0 & 0 \\ \vdots & \ddots & \vdots & \vdots \\ 0 & \dots & 0 & 0 \\ 0 & \dots & 0 & 0 \end{pmatrix}. \quad (30)$$

As has been shown above, these matrices are also sparse matrices with only one block being nonzero.

The matrices of the leads (and thus the coupling matrices as well) are infinite-dimensional matrices. We use the complex absorbing potential to truncate these matrices to form a finite-dimensional representation. In this work we will adopt the CAP suggested in [35]. This negative, imaginary CAP is derived from a physically motivated differential equation and its form is

$$-\mathrm{i}w(x) = -\mathrm{i}\frac{\hbar^2}{2m}\left(\frac{2\pi}{\Delta x}\right)^2 f(y) \quad (31)$$

where $\Delta x = x_2 - x_1$, x_1 is the start and x_2 is the end of the absorbing region, c is a numerical constant, m is the electron's mass and

$$f(y) = \frac{4}{(c-y)^2} - \frac{4}{(c-y)^2} \qquad y = \frac{c(x-x_1)}{\Delta x}. \quad (32)$$

The CAP goes to infinity at the end of the absorbing region and effectively cuts off the leads beyond that distance. The left and right CAPs are $w^{\mathrm{L}}(x)$ and $w^{\mathrm{R}}(x)$ and their starting points, x_1^{L} and x_1^{R} are deep inside the lead so the complex potential does not effect the middle region. Both the left and the right CAPs have the same range which we denote by Δx. This range typically extends over 4–6 principal layers in the lead. The accuracy of the approach can be increased by increasing the range of the complex potentials. Denoting the numbers of layers in the range of the left and right complex potentials as n_{L} and n_{R}, respectively, one only has to retain n_{L} (n_{R}) blocks in the Hamiltonian of the lead, that is the H_{L} and H_{R} become finite-dimensional matrices. If m_{L} (m_{R}) is the dimension of the block matrices of H_{L} (H_{R}) then the dimension of the Hamiltonian of the lead is $N_{\mathrm{L}} = n_{\mathrm{L}} \times m_{\mathrm{L}}$ ($N_{\mathrm{R}} = n_{\mathrm{R}} \times m_{\mathrm{R}}$). The dimension of H_{C} is N_{C}.

The matrix representations of the CAPs in the left and right leads are

$$W_{\mathrm{L}} = \begin{pmatrix} w_{n_{\mathrm{L}}}^{L} & 0 & 0 & \dots & 0 & 0 \\ 0 & w_{n_{\mathrm{L}}-1}^{L} & 0 & \dots & 0 & 0 \\ 0 & 0 & w_{n_{\mathrm{L}}-2}^{L} & \dots & 0 & 0 \\ \vdots & \vdots & \vdots & \ddots & \vdots & \vdots \\ 0 & 0 & 0 & \dots & w_2^{\mathrm{L}} & 0 \\ 0 & 0 & 0 & \dots & 0 & w_1^{\mathrm{L}} \end{pmatrix}, \quad (33)$$

$$W_{\mathrm{R}} = \begin{pmatrix} w_1^{R} & 0 & 0 & \dots & 0 & 0 \\ 0 & w_2^{R} & 0 & \dots & 0 & 0 \\ 0 & 0 & w_3^{R} & \dots & 0 & 0 \\ \vdots & \vdots & \vdots & \ddots & \vdots & \vdots \\ 0 & 0 & 0 & \dots & w_{n_{\mathrm{R}}-1}^{\mathrm{R}} & 0 \\ 0 & 0 & 0 & \dots & 0 & w_{n_{\mathrm{R}}}^{\mathrm{R}} \end{pmatrix}, \quad (34)$$

where the block matrices w_i^{L} and w_i^{R} correspond to the principal layers and thus the block matrices h_{00}^{L} and h_{00}^{R} of the Hamiltonian of the lead. In the Lagrange basis representation the CAP matrices w_i^{L} and w_i^{R} are diagonal. The matrix elements are equal to the value of the complex potential evaluated at the corresponding grid points; therefore, the matrix elements depend on the position and are different in each principal layer.

The Hamiltonian matrix using the complex potentials takes the form

$$H = \begin{pmatrix} H_{\mathrm{L}} - \mathrm{i}W_{\mathrm{L}} & H_{\mathrm{LC}} & 0 \\ H_{\mathrm{LC}}^{\dagger} & H_{\mathrm{C}} & H_{\mathrm{RC}}^{\dagger} \\ 0 & H_{\mathrm{RC}} & H_{\mathrm{R}} - \mathrm{i}W_{\mathrm{R}} \end{pmatrix}, \quad (35)$$

with finite-dimensional block matrices as has been discussed above. The Green's functions of the leads in this case can be written as

$$g_{\mathrm{L}} = \begin{pmatrix} g_{11}^{L} & g_{12}^{L\dagger} & \dots & \dots & \dots & g_{1n_L}^{L\dagger} \\ g_{12}^{L} & g_{22}^{L} & g_{23}^{L\dagger} & \dots & \dots & g_{2n_L}^{L\dagger} \\ g_{13}^{\mathrm{L}} & g_{23}^{L} & g_{33}^{L} & \dots & \dots & g_{3n_L}^{L\dagger} \\ \vdots & \vdots & \vdots & \ddots & \vdots & \vdots \\ \vdots & \vdots & \vdots & \dots & g_{n_{\mathrm{L}}-1n_{\mathrm{L}}-1}^{\mathrm{L}} & g_{n_{\mathrm{L}}-1n_{\mathrm{L}}}^{L\dagger} \\ g_{1n_{\mathrm{L}}}^{\mathrm{L}} & g_{2n_L}^{L} & g_{3n_L}^{L} & \dots & g_{n_{\mathrm{L}}-1n_{\mathrm{L}}}^{\mathrm{L}} & g_{n_{\mathrm{L}}n_{\mathrm{L}}}^{\mathrm{L}} \end{pmatrix}, \quad (36)$$

and

$$g_{\mathrm{R}} = \begin{pmatrix} g^{R}_{11} & g^{R\dagger}_{12} & \cdots & \cdots & \cdots & g^{R\dagger}_{1n_{\mathrm{R}}} \\ g^{R}_{12} & g^{R}_{22} & g^{R\dagger}_{23} & \cdots & \cdots & g^{R\dagger}_{2n_{\mathrm{R}}} \\ g^{\mathrm{R}}_{13} & g^{R}_{23} & g^{R}_{33} & \cdots & \cdots & g^{R\dagger}_{3n_{\mathrm{R}}} \\ \vdots & \vdots & \vdots & \ddots & \vdots & \vdots \\ \vdots & \vdots & \vdots & \cdots & g^{\mathrm{R}}_{n_{\mathrm{R}}-1n_{\mathrm{R}}-1} & g^{R\dagger}_{n_{\mathrm{R}}-1n_{\mathrm{R}}} \\ g^{\mathrm{R}}_{1n_{\mathrm{R}}} & g^{R}_{2n_{\mathrm{R}}} & g^{R}_{3n_{\mathrm{R}}} & \cdots & g^{\mathrm{R}}_{n_{\mathrm{R}}-1n_{\mathrm{R}}} & g^{\mathrm{R}}_{n_{\mathrm{R}}n_{\mathrm{R}}} \end{pmatrix}. \tag{37}$$

Using the leads' Green's functions and the special sparse structure of H_{LC} and H_{RC} the sigma matrices become

$$\Sigma_{\mathrm{L}} = \begin{pmatrix} h^{\dagger}_{\mathrm{LC}} g^{\mathrm{L}}_{n_{\mathrm{L}}n_{\mathrm{L}}} h_{\mathrm{LC}} & \cdots & 0 & 0 \\ 0 & \cdots & 0 & 0 \\ 0 & \cdots & 0 & 0 \\ \vdots & \ddots & \vdots & \vdots \\ 0 & \cdots & 0 & 0 \\ 0 & \cdots & 0 & 0 \end{pmatrix}, \tag{38}$$

$$\Sigma_{\mathrm{R}} = \begin{pmatrix} 0 & \cdots & 0 & 0 \\ 0 & \cdots & 0 & 0 \\ 0 & \cdots & 0 & 0 \\ \vdots & \ddots & \vdots & \vdots \\ 0 & \cdots & 0 & 0 \\ 0 & \cdots & 0 & h^{\dagger}_{\mathrm{RC}} g^{\mathrm{R}}_{11} h_{\mathrm{RC}} \end{pmatrix}, \tag{39}$$

which are both $N_{\mathrm{C}} \times N_{\mathrm{C}}$ matrices with only an $m_{\mathrm{L}} \times m_{\mathrm{L}}$ and an $m_{\mathrm{R}} \times m_{\mathrm{R}}$ nonzero block matrix.

Appendix B. Application of operators in iterative diagonalization

The Lanczos algorithm is an iterative method first proposed by Cornelius Lanczos [36] that is an adaptation of the power iteration method to find eigenvalues and eigenvectors of a square matrix (or a linear operator in general) or the singular value decomposition of a rectangular matrix. It is particularly useful for finding extreme eigenvalues of very large sparse matrices. To calculate the eigensolutions of an operator O, the Lanczos algorithm generates a set of vectors (Lanczos vectors) by a three step recursion process ($j = 1, \ldots, m$):

$$\begin{aligned} \phi_j &= O\psi_j - \beta_j \psi_{j-1} \\ \alpha_j &= \langle \phi_j | \psi_j \rangle \\ \phi'_j &= \psi_j - \alpha_j \psi_j \\ \beta_{j+1} &= \sqrt{\langle \phi'_j | \phi'_j \rangle} \\ \psi_{j+1} &= \frac{\phi'_j}{\beta_{j+1}} \end{aligned} \tag{40, 41}$$

starting with $\psi_0 = 0$, $\beta_1 = 0$ and ψ_1 is a random vector normalized to unity. After the iteration, the operator in the Lanczos vector representation take a tridiagonal form:

$$O = \begin{pmatrix} \alpha_1 & \beta_2 & & \ldots & 0 \\ \beta_2 & \alpha_2 & \beta_3 & \ldots & 0 \\ 0 & \beta_3 & \alpha_3 & \ldots & 0 \\ \vdots & \vdots & & \ddots & 0 \\ 0 & 0 & 0 & \ldots & \alpha_m \end{pmatrix}. \tag{42}$$

This tridiagonal matrix can be easily diagonalized and the lowest eigenvalues converge first. To increase the numerical stability of the algorithm vectors may be re-orthogonalized several times during the calculations.

In the Lanczos algorithm one needs to compute the action of operator O on a trial vector ψ. If the dimensionality of the basis is large, the direct storage of a matrix representation of O is not feasible. It is an important feature of the Lanczos algorithm that one only needs to store vector $O\psi$ in the calculation. Let us first examine the action of

$$(E + \mathrm{i}\epsilon^{+})I_{\mathrm{C}} - H_{\mathrm{C}} - \Sigma_{\mathrm{L}}(E) - \Sigma_{\mathrm{R}}(E) \tag{43}$$

on a wavefunction Ψ_{C}. The first term is proportional to the identity operator, the second is a multiplication with the Hamiltonian, which is a standard operation in grid type calculations. The application of the third term on the N_{C}-dimensional vector Ψ_{C} is

$$\Psi'_{\mathrm{C}} = \Sigma_{\mathrm{L}}(E)\Psi_{\mathrm{C}} = H^{\dagger}_{\mathrm{LC}} g_{\mathrm{L}}(E) H_{\mathrm{LC}} \Psi_{\mathrm{C}}. \tag{44}$$

The effect of the first operator

$$\Psi_{\mathrm{L}} = H_{\mathrm{LC}}\Psi_{\mathrm{C}}, \tag{45}$$

where Ψ_{L} is an N_{L}-dimensional vector, can be easily evaluated because only one small block of H_{LC} is nonzero. Next,

$$\Psi'_{\mathrm{L}} = g_{\mathrm{L}}(E)\Psi_{\mathrm{L}}, \tag{46}$$

where Ψ'_{L} is an N_{L}-dimensional vector, is rewritten as a linear equation

$$((E + \mathrm{i}\epsilon^{+})I_{\mathrm{L}} - H'_{\mathrm{L}})\Psi'_{\mathrm{L}} = \Psi_{\mathrm{L}}, \tag{47}$$

for the unknown Ψ'_{L}. Ψ'_{L} is then computed by solving this sparse linear equation using the conjugate gradient method [37]. The last step is to calculate the N_{C}-dimensional vector

$$\Psi'_{\mathrm{C}} = H^{\dagger}_{\mathrm{LC}}\Psi'_{\mathrm{L}}, \tag{48}$$

which is again a simple multiplication because H_{LC} is zero except for a single block matrix. The calculation on the $\Sigma_{\mathrm{R}}(E)$ part is the same using the appropriate Hamiltonians of the right side.

Now we turn to the evaluation of the action of Γ_{L}^{-1}. To do this we first rewrite Γ_{L} as

$$\begin{aligned} \Gamma_{\mathrm{L}} &= \mathrm{i}H^{\dagger}_{\mathrm{LC}}(g_{\mathrm{L}} - g^{\dagger}_{\mathrm{L}})H_{\mathrm{LC}} && (49) \\ &= \mathrm{i}H^{\dagger}_{\mathrm{LC}} g_{\mathrm{L}}((g^{\dagger}_{\mathrm{L}})^{-1} - (g_{\mathrm{L}})^{-1}) g^{\dagger}_{\mathrm{L}} H_{\mathrm{LC}} && (50) \\ &= \mathrm{i}H^{\dagger}_{\mathrm{LC}} g_{\mathrm{L}}(E - H'_{\mathrm{L}} - E - H'^{\dagger}_{\mathrm{L}}) g^{\dagger}_{\mathrm{L}} H_{\mathrm{LC}} && (51) \\ &= 2H^{\dagger}_{\mathrm{LC}} g_{\mathrm{L}} W_{\mathrm{L}} g^{\dagger}_{\mathrm{L}} H_{\mathrm{LC}}. && (52) \end{aligned}$$

Now the inverse of Γ_L becomes

$$\tfrac{1}{2} H_{LC}^{-1} g_L^{-1\dagger} W_L^{-1} g_L^{-1} H_{LC}^{-1\dagger}. \tag{53}$$

The only problematic part is the calculation of the inverse of the low rank matrix H_{LC} (to be precise, by H_{LC}^{-1} we actually mean the pseudo-inverse of H_{LC}). To calculate the effect of H_{LC}^{-1} on an N_C-dimensional vector Ψ_C, we solve the sparse linear equation

$$\Psi_C = H_{LC} \Psi_L \tag{54}$$

for the unknown Ψ_L. This can be done by a singular value decomposition,

$$H_{LC} = U W V^T, \tag{55}$$

where U is a column-orthogonal $N_L \times N_C$ matrix, V is an orthogonal $N_C \times N_C$ matrix, and W is an $N_C \times N_C$ diagonal matrix with positive or zero elements w_i (singular values) in the diagonal. Using the singular value decomposition, the solution of equation (54) is

$$\Psi_L = V \mathrm{diag}(1/w_i) U^T \Psi_C \tag{56}$$

where $1/w_i$ is replaced by zero for $w_i = 0$ [37]. As only one block of H_{LC} is nonzero, this singular value decomposition is computationally inexpensive.

The rest of the operations in equation (53) are simple. The multiplication with

$$g_L^{-1} = E I_L - H'_L \tag{57}$$

is a sparse matrix multiplication. Since W_L is diagonal, the multiplication with W_L^{-1} is simply a multiplication with the inverse of the diagonal elements.

References

[1] Datta S 1997 *Electronic Transport in Mesoscopic Systems* (Cambridge: Cambridge University Press)
[2] Faleev S V, Léonard F M C, Stewart D A and van Schilfgaarde M 2005 *Phys. Rev.* B **71** 195422
[3] Palacios J J, Pérez-Jiménez A J, Louis E, SanFabián E and Vergés J A 2003 *Phys. Rev. Lett.* **90** 106801
[4] Stokbro K, Taylor J, Brandbyge M, Mozos J L and Ordejón P 2003 *Comput. Mater. Sci.* **27** 151
[5] Emberly E G and Kirczenow G 2001 *Phys. Rev.* B **64** 235412
[6] Taylor J, Guo H and Wang J 2001 *Phys. Rev.* B **63** 245407
[7] Nardelli M B, Fattebert J-L and Bernholc J 2001 *Phys. Rev.* B **64** 245423
[8] Xue Y, Datta S and Ratner M A 2001 *J. Chem. Phys.* **115** 4292
[9] Thygesen K and Jacobsen K 2005 *Chem. Phys.* **319** 111 (Molecular Charge Transfer in Condensed Media-from Physics and Chemistry to Biology and Nanoengineering in honour of Alexander M Kuznetsov on his 65th birthday)
[10] Ke S-H, Baranger H U and Yang W 2004 *Phys. Rev.* B **70** 085410
[11] Derosa P and Seminario J 2001 *J. Phys. Chem.* B **105** 471
[12] Zhang X, Fonseca L and Demkov A 2002 *Phys. Status Solidi* b **233** 70
[13] Sanvito S, Lambert C J, Jefferson J H and Bratkovsky A M 1999 *Phys. Rev.* B **59** 11936
[14] Garcia-Lekue A and Wang L 2009 *Comput. Mater. Sci.* **45** 1016
[15] Chelikowsky J R, Troullier N, Wu K and Saad Y 1994 *Phys. Rev.* B **50** 11355
[16] Briggs E L, Sullivan D J and Bernholc J 1996 *Phys. Rev.* B **54** 14362
[17] Beck T L 2000 *Rev. Mod. Phys.* **72** 1041
[18] Varga K, Zhang Z and Pantelides S T 2004 *Phys. Rev. Lett.* **93** 176403
[19] Varga K and Pantelides S T 2007 *Phys. Rev. Lett.* **98** 076804
[20] Fujimoto Y and Hirose K 2003 *Phys. Rev.* B **67** 195315
[21] Kong L, Chelikowsky J R, Neaton J B and Louie S G 2007 *Phys. Rev.* B **76** 235422
[22] Driscoll J A and Varga K 2010 *Phys. Rev.* B **81** 115412
[23] Hirose K, Kobayashi N and Tsukada M 2004 *Phys. Rev.* B **69** 245412
[24] Khoo K H and Chelikowsky J R 2009 *Phys. Rev.* B **79** 205422
[25] Iitaka T *et al* 1997 *Phys. Rev.* E **56** 1222
[26] Paulsson M and Brandbyge M 2007 *Phys. Rev.* B **76** 115117
[27] Driscoll J A and Varga K 2008 *Phys. Rev.* B **78** 245118
[28] Sancho M P L, Sancho J M L and Rubio J 1985 *J. Phys. F: Met. Phys.* **15** 851
[29] Boyd J 2001 *Chebyshev and Fourier Spectral Methods* 2nd revised edn (New York: Dover)
[30] Cuevas J C, Yeyati A L and Martín-Rodero A 1998 *Phys. Rev. Lett.* **80** 1066
[31] Bagrets A, Papanikolaou N and Mertig I 2006 *Phys. Rev.* B **73** 045428
[32] Brandbyge M, Sørensen M R and Jacobsen K W 1997 *Phys. Rev.* B **56** 14956
[33] Strange M, Kristensen I S, Thygesen K S and Jacobsen K W 2008 *J. Chem. Phys.* **128** 114714
[34] Calzolari A, Cavazzoni C and Buongiorno Nardelli M 2004 *Phys. Rev. Lett.* **93** 096404
[35] Manolopoulos D E 2002 *J. Chem. Phys.* **117** 9552
[36] Lanczos C 1952 *J. Res. Natl Bur. Stand.* **49** 33
[37] Press W, Teukolsky S, Vetterling W and Flannery B 1992 *Numerical Recipes in FORTRAN: the Art of Scientific Computing* (New York: Cambridge University Press)